A Flexible EMI Measurement Sheet to Measure Electric and Magnetic Fields Separately with Distributed Antennas and LSI's

Naoki Masunaga, Koichi Ishida, Zhiwei Zhou, Tadashi Yasufuku, Tsuyoshi Sekitani *, Takao Someya *, Makoto Takamiya **, and Takayasu Sakurai

Institute of Industrial Science, University of Tokyo, Japan

** Quantum-Phase Electronics Center, School of Engineering, University of Tokyo, Japan*

*** VLSI Design and Education Center, University of Tokyo, Japan*

***Abstract*—A flexible 12cm×12cm EMI measurement sheet is developed to enable the measurement of the EMI distribution on the surface of the electronic devices by wrapping the devices in the sheet. The sheet includes 8×8 antenna array, 2V organic CMOS decoder, stretchable interconnects, and EMI detection LSI's (Large Scale Integrations) in 0.18μm CMOS. The distributed LSI's near the antennas enable the in-situ EMI measurement and have a potential to improve the measurement speed and accuracy. By changing the connection of the antenna to the LSI, the electric and magnetic fields are successfully measured separately. The minimum detectable magnetic field noise power was -70dBm and the maximum detectable noise frequency was 1GHz. The minimum detectable electric field noise power was -60dBm and the maximum detectable noise frequency was 700MHz.**

I. Introduction

An intra-system EMC in electronic devices (e.g. cell-phones and flat panel displays) is becoming a serious problem with the increasing density of the packaging. Fig. 1 shows a typical intra-system EMC in a cell-phone. The EMI noise generated by a digital LSI (Large Scale Integration) degrades the performance of an RF LSI. It is difficult to find the EMI generation points, because the electronic devices have the complicated three-dimensional structures. The conventional magnetic field probe with a X-Y scanning equipment [1] and the integrated array of magnetic field loop antennas in a solid board [2], however, are not applicable to the three-dimensional structures. To solve the problem, an EMI measurement sheet is proposed, which enables the measurement of the EMI distribution on the surface of the electronic devices by wrapping the devices with a sheet like the "furoshiki".

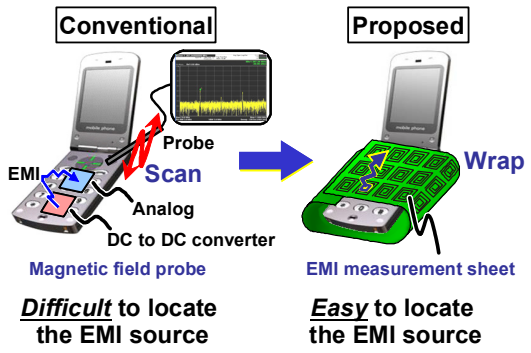

Fig. 1. Typical intra-system EMC in a cell-phone and the proposed EMI measurement sheet.

The details of the circuit techniques and the preliminary measurement results of the magnetic field by the EMI measurement sheet are shown in [3]. In this paper, the electrical field measurement by the EMI measurement sheet is newly demonstrated and the measured frequency characteristics of the EMI measurement sheet for both the magnetic and electric field are shown.

II. Flexible EMI Measurement Sheet

Fig. 2 shows a prototype of the developed EMI measurement sheet. Fig. 3 shows the block diagram of the EMI measurement sheet. The 12cm×12cm sheet has 4×4 PCB

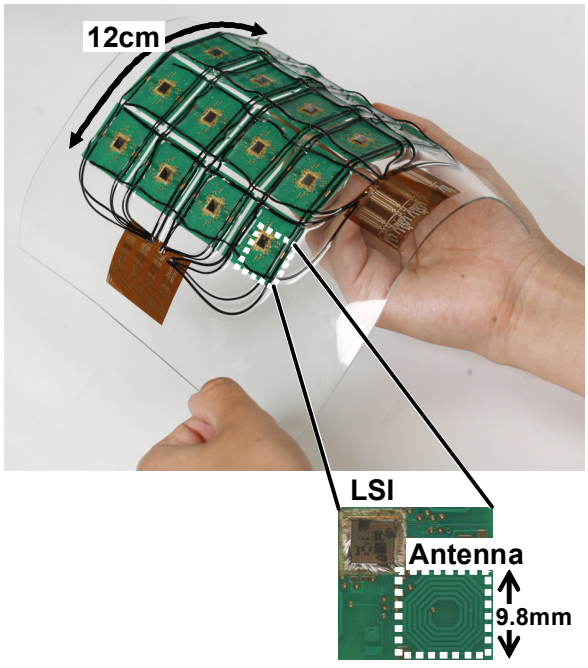

Fig. 2. Prototype of the flexible EMI measurement sheet.

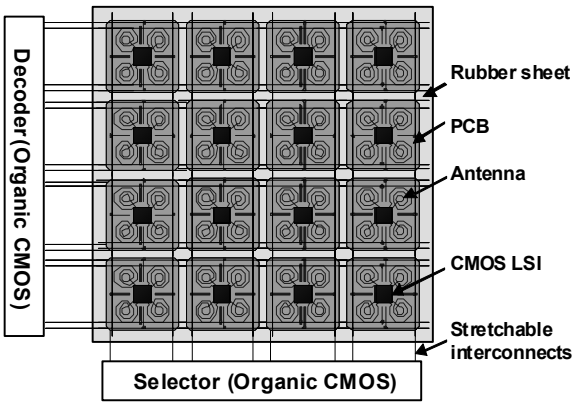

Fig. 3. Block diagram of the EMI measurement sheet.

array and 2 organic circuits (decoder and selector) on the rubber sheet made of silicone elastomer. The PCB's and the organic circuits are connected by stretchable interconnects [4] including carbon nanotubes, and the whole system is covered with a rubber sheet, which enables the sheet to be stretched.

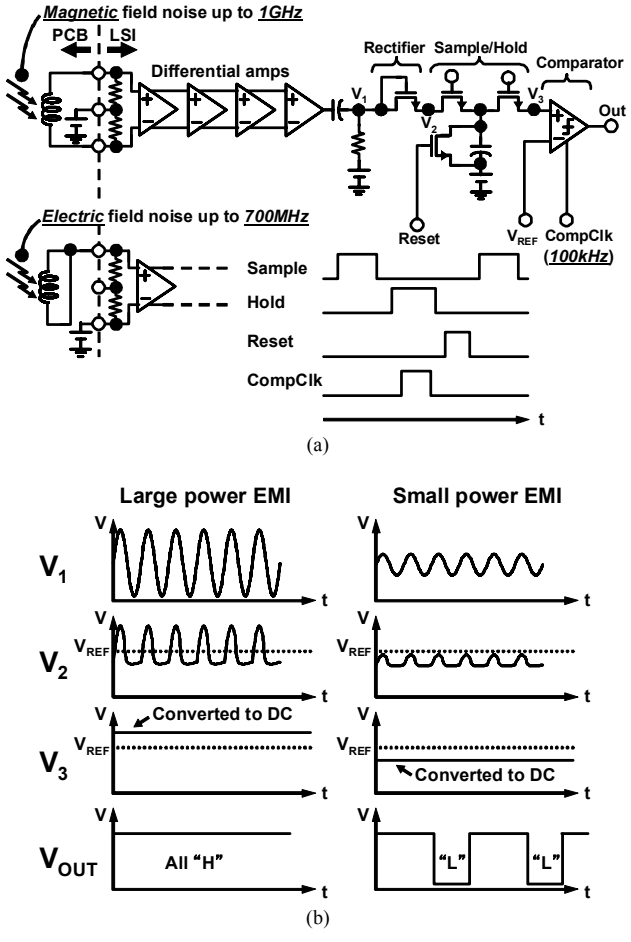

Fig. 4. (a) Circuit diagram and timing chart of the proposed EMI measurement LSI. (b) Operation of the EMI measurement LSI.

Each PCB has a 2×2 antenna array to pick up EMI, an LSI, and 6 stretchable interconnects. The 4 antennas share the LSI to measure EMI. In the conventional integrated array of magnetic field antennas in a solid board [2], the processing function of the measured results is not integrated in the board. In contrast, the EMI measurement sheet has the distributed LSI's near the antennas for the EMI measurement. It is the first demonstration of the distributed in-situ EMI measurement, which has a potential to improve the measurement speed and accuracy.

The diameter of the loop antenna is 9.8mm. The antennas are made on a rigid PCB, because the antennas on a flexible film provide unstable antenna characteristics depending on the mechanical bending.

When the scale of the array is large, a low-cost and large-area decoder is required to reduce the number of interconnects and the organic transistor are suitable for the decoder [5]. In this study, 2V organic CMOS technology enabled by the 2.1nm-thickness gate insulator (SAM[6]) and the organic semiconductor (NTCDI[7]) for nMOS was used. The measured organic decoder operation is shown in [3].

III. EMI Measurement LSI

Fig. 4(a) shows the circuit diagram and the timing chart of the proposed EMI measurement LSI. The LSI has four-stage differential amplifiers, an nMOS rectifier, sample and hold circuits, and a comparator. The conventional integrated EMI sensor circuits [8] have analog outputs, which is not suitable for the array measurement. In contrast, the developed EMI measurement LSI has a digital output, which is suitable for the array measurement.

By changing the connection method of the antenna, the electric and magnetic fields are measured separately [9]. When the both ends of the antenna are connected to the inputs of the differential amplifier, the magnetic field is measured, because the differential current in the antenna is amplified. In contrast, when the both ends of the antenna are connected to the one input of the differential amplifier and the other input of the amplifier is connected to the bias voltage, the electric field is measured, because the common-mode current in the antenna is amplified.

To capture the waveform of the EMI noise up to 1GHz

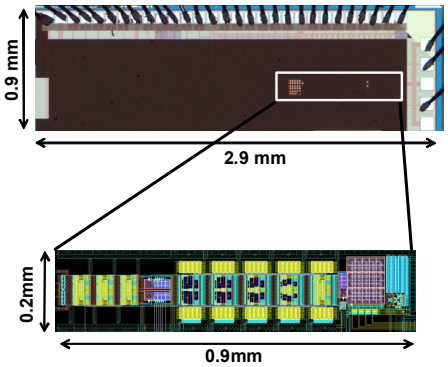

Fig. 5. Die microphotograph and layout of the EMI measurement LSI.

accurately, bandwidth of the comparator should be 10GHz or higher, which is not reasonable. The proposed LSI, therefore, converts the EMI noise waveform into the DC voltage by the rectifier and the sample and hold circuits. The down conversion relaxes the requirement for the speed of the comparator and the comparator can operate at slow frequency such as 100kHz. Fig. 4(b) shows the operation of the EMI measurement LSI. When the EMI power is large, the sampled voltage (V_3) is higher than the reference voltage (V_{REF}) of the comparator and the output of the comparator (V_{OUT}) is high. In contrast, when the EMI power is small, V_3 is lower than V_{REF} and V_{OUT} is low. The V_{OUT} is reset to high at every clock (CompClk) edge, because the comparator is a clocked comparator. In this way, the EMI noise power is observed as a function of V_{REF}.

The four-stage differential amplifiers in Fig. 4(a) have a gain of around 80dB, which enables the measurement of the magnetic EMI noise of -70dBm which equals to 45μV at 50-ohm input resistance of the amplifier.

Fig. 5 shows die microphotograph and the layout of the EMI measurement LSI. The LSI is implemented in 1.8-V, 0.18-μm CMOS process and the core area is 0.18mm^2.

IV. Measurement of Electric and Magnetic Fields

A. Comparison of Conventional and Proposed Methods

In order to demonstrate the operation of the EMI measurement sheet, the same magnetic EMI's measured with the conventional magnetic probe [1] and the developed EMI measurement sheet are compared. DUT is a memory module in a laptop PC. Figs. 6(a) and (b) show the photograph of the measurement setup and the spectrum of the measured magnetic EMI noise with the conventional magnetic probe, respectively. The highest peak was -50dBm at 267MHz.

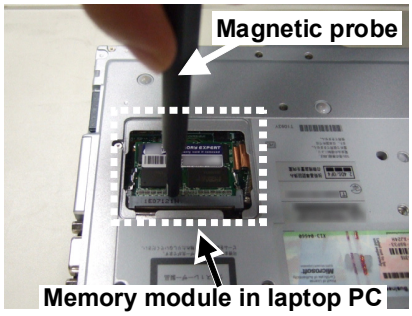

(a)

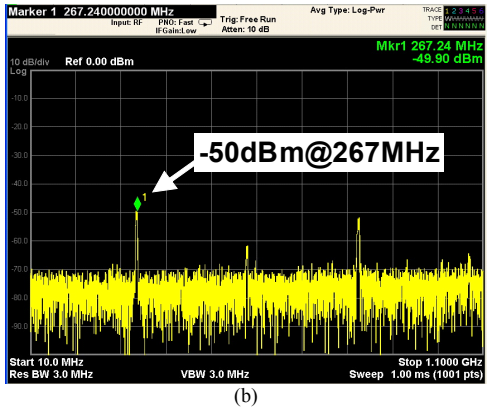

(b)

Fig. 6. Measured magnetic EMI noise with the conventional magnetic probe. (a) Measurement setup. (b) Spectrum of the noise.

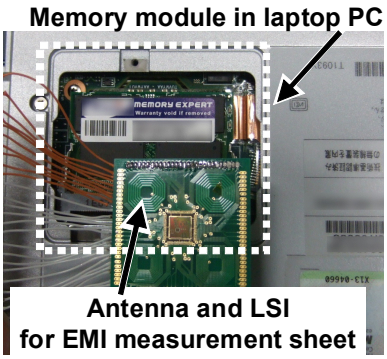

(a)

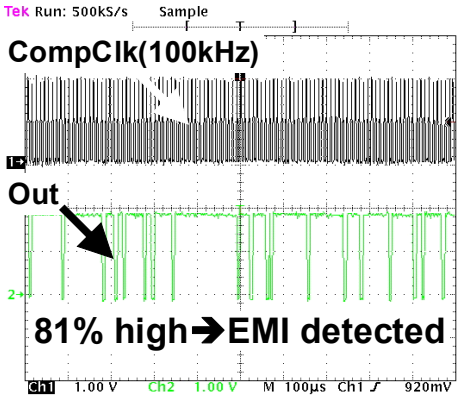

(b)

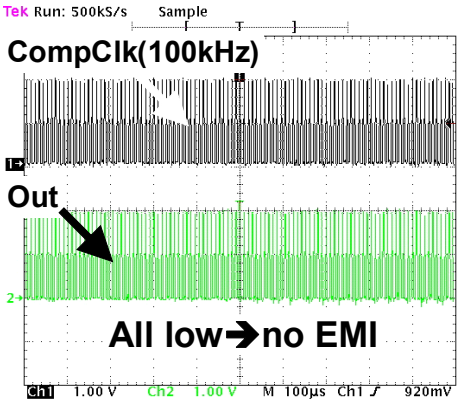

(c)

Fig. 7. Measured magnetic EMI noise with the EMI measurement sheet. (a) Measurement setup. (b) and (c) show the output waveform of the developed EMI measurement LSI with and without DUT, respectively.

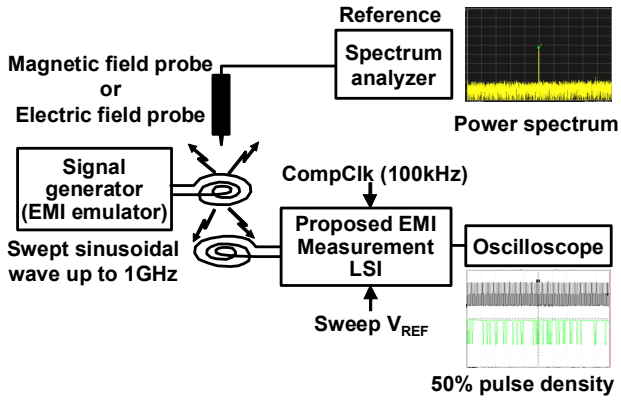

Fig. 8. Measurement setup in order to calibrate the frequency characteristics of the measurement of the electric and magnetic fields in the EMI measurement LSI.

Similarly, Fig. 7(a) shows the photograph of the measurement setup with the EMI measurement sheet. Figs. 7(b) and (c) show the output waveform of the developed EMI measurement LSI with and without DUT, respectively. In Fig. 7(b), the output shows high pulse density of 81%, which detects the EMI noise above the DUT. In Fig. 7(c), however, the output shows include no high pulse, which detects no EMI noise without the DUT. Thus, the proposed system successfully detects the actual noise emitted by the memory module in the laptop PC.

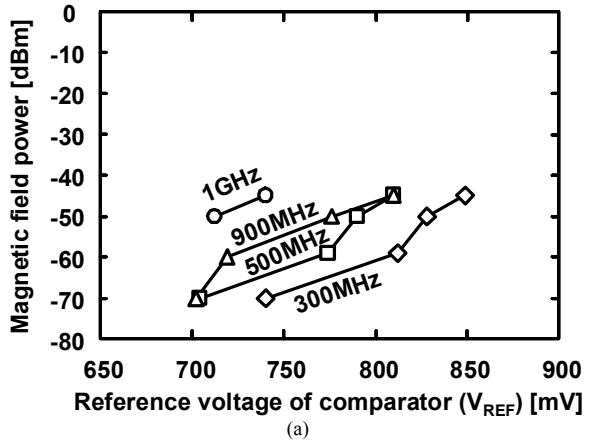

(a)

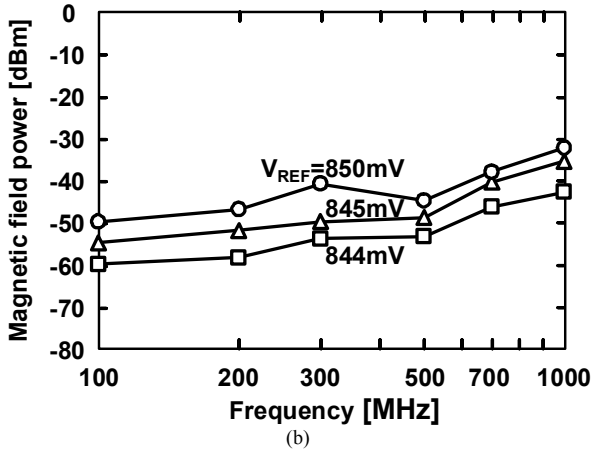

(b)

Fig. 9. Measured magnetic field power with the EMI measurement LSI. (a) V_{REF} dependence at different EMI frequency. (b) Frequency characteristics at different V_{REF}'s.

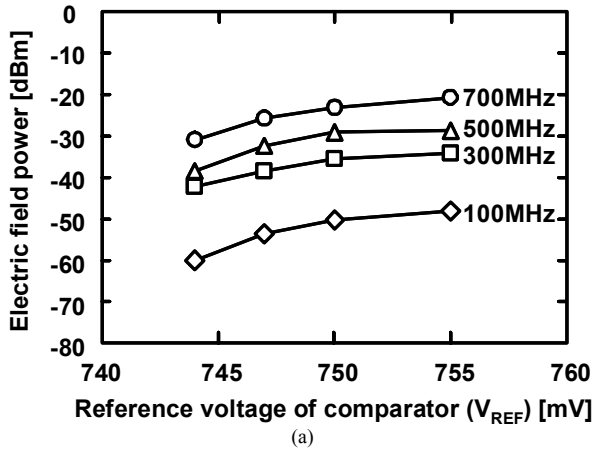

(a)

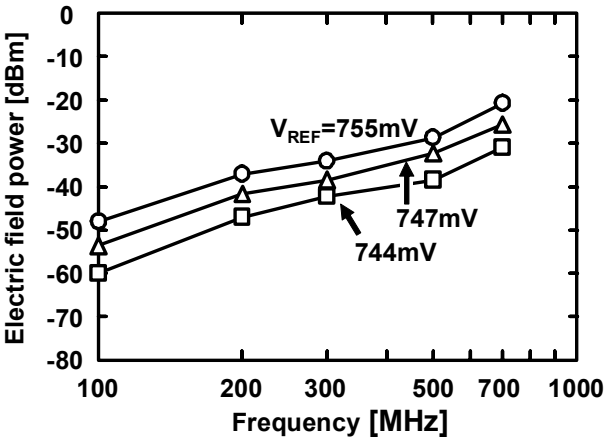

(b)

Fig. 10. Measured electric field power with the EMI measurement LSI. (a) V_{REF} dependence at different EMI frequency. (b) Frequency characteristics at different V_{REF}'s.

B. Calibration for EMI Measurement LSI

Fig. 8 shows the measurement setup in order to calibrate the frequency characteristics of the measurement of the electric and magnetic fields in the EMI measurement LSI. EMI noise is emulated by using a signal generator and an antenna. The signal generator sweeps sinusoidal wave up to 1GHz. The EMI noise is measured by the EMI measurement LSI and the commercial magnetic [1] and electric [10] field probes. The magnetic field probe detects power ranging from 10MHz to 3GHz within ±1dBuA/m error. The emulated EMI noise is monitored with the probe and the spectrum analyzer to calibrate the noise power. Similar to the magnetic field

TABLE I PERFORMANCE SUMMARY OF THE EMI MEASUREMENT LSI

Technology	1.8V, 0.18μm CMOS	
Core area	0.18mm^2	
Sampling frequency	100kHz	
Power consumption	110mW	
EMI Measurement	Magnetic field	Electric field
Minimum detectable noise power	-70dBm	-60dBm
Maximum detectable noise frequency	1GHz	700MHz

calibration, the electric field strength is calibrated by the electric field probe that can handle electric field from 2MHz to 2GHz.

Fig. 9(a) shows the measured relationship between the magnetic field power and V_{REF} at different EMI frequency in the EMI measurement LSI. V_{REF} increases with increasing the magnetic field power. The minimum detectable magnetic field noise power was -70dBm. Fig. 9(b) shows the measured frequency characteristics of the magnetic field power at different V_{REF}'s. The maximum detectable noise frequency was 1GHz. Ideally, the frequency characteristics should be flat. The magnetic field power, however, increases with increasing the frequency, which derives from the frequency characteristics of the amplifier in the EMI measurement LSI.

Similarly, Fig. 10(a) shows the measured relationship between the electric field power and V_{REF} at different EMI frequency and Fig. 10(b) shows the measured frequency characteristics of the electric field power at different V_{REF}'s. The minimum detectable electric field noise power was -60dBm and the maximum detectable noise frequency was 700MHz.

Comparing the electric and magnetic fields measurement shown in Figs. 9(a) and 10(a), the sensitivity of the electric fields measurement is worse than that of the magnetic fields measurement. The difference derives from the antenna gain difference between the electric and magnetic fields.

Key features of the developed the EMI measurement LSI are summarized in Table I.

V. CONCLUSION

Collaboration among silicon CMOS technology, 2V organic CMOS technology, and stretchable interconnect including carbon nanotubes makes a stretchable EMI measurement sheet possible, and the proposed LSI demonstrates EMI noise measurement up to 1GHz by using rectifier and the comparator operating at only 100kHz. By changing the connection of the antenna to the LSI, the electric and magnetic fields are successfully measured separately. The minimum detectable magnetic field noise power was -70dBm and the maximum detectable noise frequency was 1GHz. The minimum detectable electric field noise power was -60dBm and the maximum detectable noise frequency was 700MHz.

ACKNOWLEDGMENT

This work was partially supported by the Grant-in-Aid for Scientific Research, Special Coordination Funds for Promoting and Technology, NEDO, and CREST/JST.

REFERENCES

[1] Magnetic probe (CP-2S), NEC Corporations.
[2] EMSCAN. [Online]. Available: http://emscan.com/
[3] K. Ishida, N. Masunaga, Z. Zhou, T. Yasufuku, T. Sekitani, U. Zschieschang, H. Klauk, M. Takamiya, T. Someya, and T. Sakurai, "A stretchable EMI measurement sheet with 8×8 coil array, 2V organic CMOS decoder, and -70dbm EMI detection circuits in 0.18um CMOS," *IEEE International Solid-State Circuits Conference*, Feb. 2009. (to be presented)
[4] T. Sekitani, Y. Noguchi, K. Hata, T. Fukushima, T. Aida, and T. Someya, "A rubberlike stretchable active matrix using elastic conductors," *Science*, vol. 321, pp. 1468-1472, Sep., 2008.
[5] T. Someya, H. Kawaguchi, and T. Sakurai, "Cut-and-paste organic FET customized ICs for application to artificial skin," *IEEE International Solid-State Circuits Conference*, pp. 288-289, Feb. 2004.
[6] H. Klauk, U. Zschieschang, J. Pflaum, and M. Halik, "Ultralow-power organic complementary circuits," *Nature*, vol. 445, pp. 745-748, Feb., 2007.
[7] H. E. Katz, A. J. Lovinger, J. Johnson, C. Kloc, T. Siegrist, W. Li, Y.-Y. Lin, and A. Dodabalapur, "A soluble and air-stable organic semiconductor with high electron mobility," *Nature*, vol. 404, pp. 478-481, Mar., 2000.
[8] S. Aoyama, S. Kawahito, T. Yasui, and M. Yamaguchi, "A high-sensitivity active magnetic probe using CMOS integrated circuits technology," IEEE Topical Meeting on Electrical Performance of Electronic Packaging, pp.103-106, Oct. 2005.
[9] S. Kazama and Ken Ichi Arai, "Adjacent electric field and magnetic field distribution measurement system," IEEE International Symposium on Electromagnetic Compatibility, vol. 1, pp. 395-400, Aug. 2002.
[10] Credence Technologies. [Online]. Available: http://www.credencetech.com/products/product.php?productId=CTK031